Published in final edited form as:
ACS Nano. 2009 March 24; 3(3): 585–594. doi:10.1021/nn800863w.

Ultrasensitive Immunosensor for Cancer Biomarker Proteins using Gold Nanoparticle Film Electrodes and Multienzyme-Particle Amplification

Vigneshwaran Mani[†], **Bhaskara V. Chikkaveeraiah**[†], **Vyomesh Patel**[‡], **J. Silvio Gutkind**[‡], and **James F. Rusling**[*,†,§,ζ]

†*Department of Chemistry, 55 N. Eagleville Rd., University of Connecticut, Storrs, Connecticut 06269*

‡*Oral and Pharyngeal Cancer Branch, National Institute of Dental and Craniofacial Research, National Institutes of Health, Bethesda, Maryland 20892.*

§*Department of Cell Biology, University of Connecticut Health Center, Farmington, CT 06032*

ζ*Institute of Materials Science, University of Connecticut, Storrs, Connecticut 06269*

Abstract

A densely packed gold nanoparticle platform combined with a multiple-enzyme labeled detection antibody-magnetic bead bioconjugate was used as the basis for an ultrasensitive electrochemical immunosensor to detect cancer biomarkers in serum. Sensitivity was greatly amplified by synthesizing magnetic bioconjugates particles containing 7500 horseradish peroxidase (HRP) labels along with detection antibodies (Ab_2) attached to activated carboxyl groups on 1 μm diameter magnetic beads. These sensors had sensitivity of 31.5 μA mL ng^{-1} and detection limit (DL) of 0.5 pg mL^{-1} for prostate specific antigen (PSA) in 10 μL of undiluted serum. This represents an ultralow mass DL of 5 fg PSA, eight fold better than a previously reported carbon nanotube (CNT) forest immunosensor featuring multiple labels on carbon nanotubes, and near or below the normal serum levels of most cancer biomarkers. Measurements of PSA in cell lysates and human serum of cancer patients gave excellent correlations with standard ELISA assays. These easily fabricated AuNP immunosensors show excellent promise for future fabrication of bioelectronic arrays.

Keywords

gold nanoparticles; immunosensor; cancer biomarkers; multilabel amplification

Gold nanoparticles (AuNPs) exhibit quantum size effects leading to unique optical, electronic, and catalytic properties.[1–7] They are fully compatible[8,9] with biomolecules when decorated with thin organic coatings. This has resulted in their use in sensors for DNA,[10,11] proteins,[12] organic analytes and metal ions.[13] Nanoscale structures of AuNPs on conductive surfaces combined with high electrical conductivity can facilitate fast electron transfer to and from redox enzymes, which has been demonstrated for cytochrome c,[14] horseradish peroxidase,[15] myoglobin[16] and glucose oxidase,[17] providing a sensitive platform for biosensors.

AuNPs have been employed as nanoelectrode[18] relay units transporting electrons from a FAD enzyme cofactor to a macroscopic electrode, efficiently activating enzyme bioelectrocatalysis. Zayats et al.[19] demonstrated electrical connection of pyrroloquinoline quinone (PQQ)-

•address correspondence to james.rusling@uconn.edu.

dependent enzymes by the reconstitution of apo-glucose dehydrogenase on PQQ functionalized AuNPs assembled on a Au underlayer. In addition, biosensors utilizing multilayer films produced layer-by-layer from polyions, gold nanoparticles, multi-wall carbon nanotubes (MWCNT) and enzymes have been evaluated.[2] Shipway et al.[20] constructed gold nanoparticle electrodes for the fabrication of devices such as sensors and photo- or bio-electrochemical devices with high sensitivity, selectivity and functionality. Modified AuNP electrodes have very large surface areas, are simple to fabricate and functionalize, retain metallic conductivity, and lend themselves to facile biomolecule attachment.[21,22] Recently Singh et al.[23] reported electrochemical immunosensors for detecting osteoproteogerin based on a AuNP-conducting polymer electrode showed a linear range from 2.5 pg mL^{-1} to 25 pg mL^{-1} with detection limit of 2 pg mL^{-1}. In this paper, we report monolayer AuNP electrodes as immunosensors that do not require conductive polymer and have significantly better detection limits for proteins in serum.

Sensitive quantitative detection of protein biomarkers is critical to many areas of biomedical research and diagnostics,[24] systems biology[25] and proteomics.[26] Biomarker levels in serum, for example, can detect and monitor diseases such as cancer.[27] Conventional ways of measuring proteins include enzyme-linked immunosorbent assays (ELISA),[28] radioimmunoassay (RIA),[29] electrophoretic immunoassay[30] and mass spectrometry-based proteomics.[31] These techniques often involve sophisticated instrumentation, significant sample volumes, limited sensitivity, and clinically unrealistic expense and time. Thus, there is a real need for simple, rapid, sensitive and inexpensive methods for protein measurement for point-of-care and research applications. For example, measurement of collections of protein cancer biomarkers promises reliable statistics for early cancer detection.[32–34] For point of care applications, these sensors need to be inexpensive, simple operationally, capable of rapid multiplexed protein detection, and have good enough sensitivity and detection limits to address both levels of the biomarkers normal and cancer patient serum. Several approaches simpler than LC-MS have been reported to measure protein biomarkers, including surface plasmon resonance,[10] carbon nanotube-based immunosensors,[35] microcantilevers,[36] nanowire transistor arrays,[37] and nanocrystals[38] all of which may be amenable to multiplexing.

The protein prostate specific antigen (PSA) in human serum is clinically measured as a biomarker for prostate cancer.[39] We recently reported high sensitivity electrochemical immunosensors applied to the detection of PSA.[40] These sensors were based on upright single wall carbon nanotube (SWNTs) forests,[41] and employed a sandwich format in which a primary antibody attached to the SWNT ends captures the protein analyte from the sample. After washing and blocking of non-specific binding, a labeled detection antibody is added to develop the signal. The most sensitive detection of PSA was achieved when signals were amplified by using separate multi-wall carbon nanotubes (MWCNTs) with a cargo of multiple enzyme labels and detection antibodies in place of conventional singly labeled detection antibodies.[40] This approach provided a detection limit (DL) of 4 pg mL^{-1} for PSA in serum and tissue lysates. While SWNT forest sensors gave excellent detection limits, problems to be overcome in multiplexed systems include nanotube heterogeneity, purification, stability, further improvement of sensitivity, and reproducibility and complexity of forest fabrication.[42]

In this paper, we report the design and evaluation of an alternative approach for electrochemical protein immunoassays employing platforms featuring densely packed 5 nm AuNPs. These sensor platforms are easy to fabricate and process, and can be produced pre-equipped with a functional organic layer for capture antibody attachment. For sensor fabrication, alternate layer-by-layer electrostatic adsorption[43,44] was used to assemble a dense glutathione-decorated AuNP[45] layer on an underlying layer of cationic poly (diallyldimethyl ammonium chloride) deposited on a pyrolytic graphite electrode. We first characterized the biocatalytic properties of these AuNP electrodes by covalently linking HRP via amidization to the

carboxylate groups of the glutathiones on the AuNP surface and measuring biocatalytic activity for detection of hydrogen peroxide at high sensitivity. We then attached a capture antibody (Ab_1) to the AuNP electrodes to detect PSA in serum. Highly amplified detection was achieved by using multi-label bioconjugates made by linked multiple horseradish peroxidase (HRP) and detection antibodies (Ab_2) to carboxylated 1.0 μm magnetic beads for signal development. This approach provided an unprecedented detection limit (DL) of 0.5 pg mL^{-1} for PSA in 10 μL undiluted serum, which is near or below the normal levels of most cancer biomarker proteins in human serum,[46] and 8-fold better than our previous SWNT forest immunosensors.

RESULTS

Fabrication and Characterization of AuNP platform

Glutathione-protected gold nanoparticles (GSH-AuNP) were prepared by a reported method, [45] then characterized by TEM and spectroscopy. TEM analyses (Supporting Information, Figure S1ab) revealed a relatively monodisperse solution with average particle diameter of 5.0 ±1.4 nm. Particle size was confirmed by visible absorption spectroscopy band for the GSH-AuNP dispersion at 508 nm indicating diameter ~4 nm (Supporting Information, Figure S1c). [47] The presence of glutathione on the AuNPs was confirmed by observation of characteristic N-H and carbonyl bands at 1538, 1628 and 1717 cm^{-1} by IR spectroscopy (Supporting Information, Figure S1d).

The sensor platform was fabricated by first adsorbing a layer of cationic polydimethyldiallylammonium (PDDA) from aqueous solution onto a pyrolytic graphite (PG) disk electrode, washing with water, then adsorbing a layer of the negatively charged 5 nm GSH-AuNPs from a dispersion (see methods) onto the PDDA, utilizing the standard layer-by-layer (LbL) alternate electrostatic adsorption approach.[44] Assembly of the PDDA/GSH-AuNP films was monitored at each step with a quartz crystal microbalance (QCM) by making films on 9-MHz gold-coated QCM resonators that were treated with 3-mercaptopropanoic acid (MPA) to mimic the partly negative PG surface before adsorbing the layers.[48] Adsorbed mass per unit area (M/A) of each layer for dried films was obtained from the measured QCM frequency change (ΔF) and the Sauerbrey equation.[43] Table 1 provides estimates of mass/unit area of AuNPs adsorbed on PDDA and the thickness of the AuNP layer. A 75% nominal surface coverage of AuNPs on the electrode was estimated based on the QCM data and the bulk density of gold. However, molecular simulations suggest that fully coated alkylthiol-gold nanoparticles have densities less than that of bulk gold,[49] possibly considerably less for the 5 nm GSH-AuNPs. A density smaller than bulk gold suggests that the 75% coverage estimated from QCM is a lower limit. For example, if the density of the 5 nm GSH-AuNPs is 85% of bulk gold, the estimated coverage increases to 100%.

Films were grown on smooth cleaved mica surfaces for characterization by atomic force microscopy. The initial thin layer of PDDA (0.5 ± 0.2 nm) adsorbed was relatively smooth with mean surface roughness of 0.13 ± 0.08 nm, almost twice that of the bare mica with 0.083 ± 0.009 nm mean surface roughness. Figures 2b,c show an AFM image that changed in topography after AuNPs were adsorbed onto the PDDA layer. A densely packed nanoparticulate layer was observed which can be associated with the AuNPs, consistent with the view that the 75% nominal surface coverage from QCM is a lower limit, The AFM data suggest that the AuNPs achieved nearly complete coverage on the underlying surface with a mean surface roughness of 1.99 ± 0.11 nm, about a 24-fold increase in surface area over the bare mica. Sectional analysis of AFMs of the AuNP platform showed that the average width of the major feature was 6.3±2.2 nm, which is well correlated with the 7 nm layer thickness obtained from QCM (Table 1) and the 5.0±1.4 nm particle diameter from TEM. Figure 2c shows the phase contrast image of the AuNP layer which is based on contrasting stiffness, viscoelasticity and chemical composition of the surface. This image is also consistent with

nearly full coverage of the solid surface with AuNPs, Figure 2d shows an AFM image after the capture antibody to PSA was covalently linked onto the carboxylates of the AuNP layer using EDC/NHSS chemistry (see Methods). The densely packed AuNP layer disappeared and a rolling hill-like appearance generally characteristic of any globular protein coated on a rough surface was observed.[35,42]

Electrochemical characterization of AuNP electrodes revealed basic electrode characteristics and the potential for biocatalytic applications. Cyclic voltammetry (CV) showed no significant oxidation or reduction peaks for PDDA adsorbed on pyrolytic graphite (PG) in the range 0.2 to −0.5 V vs SCE (Figure 3a). Addition of the AuNPs onto the PDDA layer resulted in a large increase in charging current over the entire voltage range (not shown) consistent with the large increase in surface area observed by AFM. The electrochemical surface area was found to be 0.18 cm^2 for AuNP electrode which was estimated using Randles-Sevcik equation from the slope of peak currents of soluble 1 mM ferrocyanide in 0.1 M KCl vs $\nu^{1/2}$. The presence of AuNPs on electrode resulted in an increase in surface area by 28.5% over underlying rough pyrolytic graphite and 44.8% on a polished glassy carbon surface. These increases in roughness are not as large as found on smooth mica, since the carbon electrode surfaces have much more inherent roughness. Addition of 0.2 mM H_2O_2 to the buffer gave a small increase in CV current in the negative potential range that most likely reflect the onset of peroxide reduction (Figure 3a).

Bioelectronic quality control experiments for the nanostructured electrodes[35] was done by attaching horseradish peroxidase (HRP) onto the carboxylated AuNP layer by amidization. These HRP-AuNP electrodes were used to observe the sensitivity and detection limit for the electrochemical determination of hydrogen peroxide. First, cyclic voltammograms showed a characteristic reversible reduction-oxidation peak pair of the Fe^{III}/Fe^{II} redox couple of HRP[50] at about −0.3 V shown in Figure 3b in the absence of peroxide. Surface concentration of HRP was obtained by integrating the reduction peaks and gave 0.076 ± 0.019 nmol cm^{-2}. Addition of 0.2 mM H_2O_2 to the buffer resulted in disappearance of the oxidation peak and increase in catalytic reduction peak (Figure 3b) which is characteristic of the enzyme-catalyzed electrochemical reduction.[51] Qualitatively similar results were found for HRP attached to single wall nanotube forest electrodes. [35]

Addition of H_2O_2 to HRP converts the iron heme peroxidase enzyme to a ferryloxy species that can be electrochemically reduced directly by the electrode.[50] H_2O_2 was detected via this approach on the HRP-AuNP sensors with excellent sensitivity and detection limit by using rotating disk amperometry. Applied potential of −0.2 V vs SCE and rotation rate of 2000 rpm were optimum parameters that gave the best sensitivity. Increase in H_2O_2 concentrations by 200 nM gave an increased steady state current of tens of nanoamperes for electrodes with HRP attached to AuNP platform (Figure 4a). A detection limit of 20 nM H_2O_2 was measured by injecting very small amounts of H_2O_2 until steady state current was 3 times the average noise.

Results illustrated by Figure 4a showing the amperometry resulted in a calibration curve of steady state current vs. concentration revealing a sensitivity (slope) of 0.28 μA μM^{-1} H_2O_2 (Figure 4b). This plot of steady state current vs [H_2O_2] was linear up to ~2 μM peroxide. It is of interest that addition of a second PDDA/AuNP layer to the electrode before attachment of the enzyme gave no improvement in sensitivity or detection limit. The performance of the HRP-AuNP sensors was better than previously used HRP-SWNT forests on similar PG underlayers which gave a detection limit of 40 nM and sensitivity of 0.18 μA μM^{-1} H_2O_2.[35]

AuNP immunoassay using Ab_2-HRP

The serum concentration of prostate specific antigen (PSA) is an established clinical tool for diagnosing and monitoring prostate cancer. Levels of 4 to 10 ng mL^{-1} suggests the possibility

of prostate cancer.[52] The immunosensor for PSA constructed on the AuNP platform is illustrated by Figure 1, in which we attached anti-PSA antibody by amidization onto the carboxylated AuNPs. Inhibition of nonspecific binding (NSB) of labeled detection antibodies was crucial to achieve high sensitivity and low detection limits. We optimized an effective NSB blocking procedure utilizing treatment of the immunosensors with 0.4 % Casein and 0.05 % Tween-20 in PBS buffer. After this step, PSA standards in undiluted calf serum were incubated with the AuNP immunosensors. Then, the sensor with bound PSA was finally incubated with detection anti-PSA antibody (Ab_2) labeled with horseradish peroxidase or multi-labeled Ab_2-magnetic bead bioconjugates. After several washing steps with PBS Tween-20 and PBS buffer the sensor assembly was then placed into an electrochemical cell containing 1 mM hydroquinone as mediator in PBS buffer, and hydrogen peroxide was injected to 0.4 mM while measuring the current to develop an amperometric signal proportional to PSA.

Figure 5 shows that the amperometric current from the sensor reached a steady state response rapidly, which increased linearly with PSA concentration between 1 and 40 ng mL^{-1}. Excellent sensor-to-sensor reproducibility is illustrated by the small error bars in Figure 5B, and sensitivity of 18 nA-mL ng^{-1} was achieved with linearity extending through the critical 4–10 ng mL^{-1} PSA range. Response for the immunosensors taken through the full procedure without exposure to PSA reflects the sum of residual NSB and direct reduction of H_2O_2. Signals corresponding to immunosensors built on a PG surface with no AuNP were 50% smaller than the full AuNP sensors for test concentration of 10 ng mL^{-1} (Figure 5A), showing that the use of the densely packed AuNPs provides significant enhancement of the amperometric signal.

Amplification with multilabel Ab2-magnetic bead-HRP

We attached multiple HRP labels to carboxyl groups on the magnetic bead surfaces to amplify sensitivity and improve the detection limit. HRP and Ab_2 at a 120/1 HRP/Ab_2 molar ratio was reacted with the carboxylated magnetic beads using the usual EDC amidization protocol.[40] Carboxylic acid groups were first activated using EDC, excess reagent was removed by washing with water, and the activated particles were then reacted with amine residues on the proteins. Magnetic beads of diameter ~ 1 μm provided a very high number of labels on the surface, and gave better sensitivities and detection limits for PSA than 130 nm diameter magnetic beads bioconjugated in the same fashion. After the bioconjugation of HRP and Ab_2, the free antibodies and HRP were easily separated from the Ab_2-magnetic bead-HRP by using a magnet to localize the beads at the bottom of a test tube and washing to remove unreacted protein.

The amount of active HRP per unit weight of magnetic beads was determined by reacting the Ab_2-magnetic bead-HRP dispersion with HRP substrate 2,2'-azino-bis-(3-ethylbenz-thiazoline-6-sulfonic acid) (ABTS) and H_2O_2.[53] The reaction produces a soluble product with characteristic optical absorbance band at 405 nm. The concentration of active HRP in the stock Ab_2-magnetic bead-HRP dispersion was determined by these enzyme activity experiments to be 2.18 μg mL^{-1}. Thus, the amount of active HRP was 50 pmol HRP mL^{-1} of stock dispersion. The total number of magnetic beads of ~1 μm diameter was $4*10^9$ in the dispersion provided by Polysciences, and the number of active HRP per magnetic bead was estimated at 7500.

Amperometric detection of PSA in undiluted calf serum using Ab_2-magnetic bead-HRP bioconjugates with the AuNP immunosensor is shown in Figure 6. Sensitivity and detection were improved significantly compared to when the conventional single label Ab_2-HRP was used in the immunoassay. Sensitivity as slope of the calibration curve in Figure 6B was 31.5 μA-mL ng^{-1}, ~1700 times larger than when using the conventional Ab_2-HRP with the AuNP immunosensors. The detection limit measured as 3 times the average noise above the zero PSA control was 0.5 pg mL^{-1}, 2000-fold better than the value of 1000 pg mL^{-1} using the conventional Ab_2-HRP.

Control experiments shown in Figure 6A showed that the signal from immunosensors based on bare PG or PG coated with PDDA was 5-fold smaller than that of the full AuNP immunosensor, again showing the advantage of the AuNPs on the sensor electrodes. The response for the AuNP immunosensor taken through the full procedure without exposure to PSA reflects the direct reduction of H_2O_2 and residual NSB of the Ab_2-magnetic bead-HRP bioconjugate that controls the detection limit, and is somewhat larger with the multilabel (Figure 6A) than that of single label detection (Figure 5A). However, this effect is overwhelmed by the much larger sensitivity achieved with the multilabel detection.

PSA in cell lysates and human serum samples

A collection of 2 cell lysates and 3 human serum samples were used to assess the accuracy of the AuNP sensor in real biomedical situations. PSA measurement in the range 4 to 10 ng/mL is generally regarded as suggesting a significant probability of the presence of prostate carcinoma.[54] We tested two cell lysates, one from cells which overexpress PSA[55] (LNCaP cells) and another from a non-prostate specific cell line which does not (HeLa cells).[56] Results in Figure 7A are shown along with PSA standards in calf serum at comparable concentration ranges. Three patient serum samples with varying PSA content were also tested. These samples were also assayed by a standard ELISA method (Figure 7B), where the results were represented in logarithmic form and compared on the same graph. Immunosensor results showed a very good correlation with ELISA from the sub ng mL^{-1} concentration range to above 10 ng mL^{-1} for this representative cell lysate and serum sample set. There was no significant difference in values from the two methods at the 95% confidence level for any of these samples as shown by t-tests. In addition, the HeLa cell lysate as a negative control showed levels well below 0.01 ng mL^{-1} PSA, while the positive control LNCaP cell lysates gave levels on the order of 2 ng mL^{-1} consistent with their known PSA expression. In addition, serum sample 1 from a normal human female gave a value below 1 ng mL^{-1} as expected, while serum sample 2 and 3 from males with suspected prostate carcinoma gave much larger values.

DISCUSSION

Results described above demonstrate the utility of gold nanoparticle-based immunosensors combined with amplified multilabel detection using magnetic beads for ultrasensitive detection of protein biomarkers. For the test biomarker PSA, accuracy of these immunosensors was demonstrated by the successful analysis of cell lysates and human serum samples (Figure 7), giving good agreement with the referee ELISA method. PSA determinations in these real samples did not require multilabel detection, and could be analyzed by using a conventional Ab_2-HRP bioconjugate.

Since a significant number of biomarkers have normal levels in the low pg mL^{-1} range,[46] we wished to demonstrate detection limits in this range so as to have a sensor capable of measuring both normal representative of cancer-free patients and elevated levels indicative of cancer. The approach utilizing Ab_2-magnetic bead-HRP with multiple HRP labels conferred the best sensitivity, and a detection limit of 0.5 pg mL^{-1}. It should be readily adaptable to cancer biomarkers having very low normal levels. The 0.5 pg mL^{-1} DL in 10 μL samples translates to a 5 fg mass detection limit, lower than the best commercial immunoassays[57–59]

The 0.5 pg mL^{-1} DL for PSA for AuNP sensors was improved by the multilabel Ab_2-magnetic bead-HRP from 1000 pg mL^{-1} obtained for the conventional single label Ab_2-HRP. This 2000 fold increase in DL was possible because of the 7500 HRP labels on each Ab_2-magnetic bead. In addition, the present approach improved the detection limit by 8-fold and the sensitivity by 4-fold compared to our previously developed single-wall nanotube forest immunosensors utilizing multiwall carbon nanotubes (MWCNTs) bearing multiple enzyme labels and detection antibodies.[40] A major factor in increased sensitivity and improved detection limit is

likely to be the number of HRPs bound per bead in the labeling development step, which was 7500/1 μm bead with the magnetic beads and 1700 per 1 μm nanotube length for nanotube immunosensor system. However, AuNP properties are also important since bioelectronic characterization (Figure 4) also showed two-fold improvements in sensitivity and detection limits for detection of H_2O_2 for the HRP-AuNP electrodes compared to HRP-SWNT forests in assays that did not employ any labels.

Other advantages of the magnetic beads for multiple labeling include a more narrow and reproducible size distribution than nanotubes, and ease of preparation of the labeled bioconjugates, featuring magnetic separation of Ab_2-magnetic bead-HRP from unbound proteins by using a magnet. It is possible that the sensitivity can be improved by further optimizing Ab_2-magnetic bead-HRP properties and by decreasing the NSB of this bioconjugate.

The increased density of the conductive AuNPs greatly increases the active surface area for capture antibody attachment to flexible glutathione tethers and may also be an important factor for improved sensitivity. The key advantages for higher amperometric signals include densely packed, patternable conductive nanoparticles resulting in a high surface area, highly conductive platform with protruding functional groups that allow simple bioconjugation to large amounts of primary antibodies. The immunosensors required mediation for the best sensitivity. This is most likely related to distances between the HRP labels and AuNPs that limit the efficiency of direct electron transfer.

It is important for future development that gold nanoparticle electrodes are easy to prepare and may be more easily fabricated than carbon nanotubes into arrays by automatic processing for multiple biomarkers, e.g. with ink jet spotters. Enzyme-linked immunosorbent assay (ELISA) based on optical absorbance is an important bioanalysis method with claimed DLs as low as 3 pg/mL for PSA.[60] However, ELISA suffers limitations in analysis time, sample size, and multiplexing. Preliminary studies in our laboratories suggest good potential for nanoparticles to make bioelectronic sensor array platforms to measure collections of cancer biomarkers simultaneously, at high sensitivity and without compromising analysis time or sample size. A recent study reported[61] Si-nanowire based structures configured as field effect transistors to achieve a detection limit of 1 fg mL^{-1} PSA using conductance changes associated with the binding of PSA with anti-PSA antibodies on the nanowire. This is the best detection limit claimed so far for bioelectronic PSA measurement, but PSA was detected in buffer rather than in serum and no real samples were analyzed so accuracy is unknown. In the best DL for serum using Si-nanowires, an array was used to achieve a DL of 0.9 pg mL^{-1}.[37] However, these Si nanowire transistors currently require much more sophisticated and complex fabrication procedures than the AuNP electrode platforms. In other developments,[62] scanning tunneling microscopy (STM) based electrical detection achieved a detection of 10 fg mL^{-1} for PSA in buffer using changes in electrical tunneling current which depended on bound gold nanoparticle-antibody complexes. However, STM detection in its present form could be too complex and expensive for point-of-care applications. Furthermore, detection limits very much smaller that 100 fg mL^{-1} may not be required for cancer detection since normal levels of most cancer biomarkers are well above this. Thus, the AuNP platform we describe here is competitive with other state of the art approaches in sensitivity and DL for real samples, and may prove to have clear economic advantages in future array fabrication.

In summary, we have demonstrated for the first time the combination of a densely packed gold nanoparticle platform and a multilabeled detection antibody-magnetic bead bioconjugate for the construction of an ultrasensitive electrochemical immunosensor for cancer biomarkers proteins. The biomarker PSA was accurately detected in representative biomedical samples. We are currently exploiting the ease of fabrication and proccessability of AuNP platforms

combined with high sensitivity, reproducibility, and reliability for the translation of multiplexed biomarkers detection into array formats.

METHODS SECTION

Chemicals and Materials

L-Gluthathione reduced (99%), gold (III) chloride trihydrate (99.9%) and sodium borohydride (99%) 2,2'-azino-bis(3-ethylbenzthiazoline- 6-sulfonic acid), poly (diallydimethylammonium chloride) (PDDA), horseradish peroxidase (HRP, MW 44,000) and prostate specific antigen (PSA) were from Sigma. Monoclonal (Mouse) primary anti-human PSA antibody (clone no. CHYH1), detection anti-PSA antibody (clone no. CHYH2) with and without HRP conjugation were from Anogen/Yes Biotech Lab, Ltd. 1-(3-(dimethylamino)- propyl)-3-ethylcarbodiimide hydrochloride (EDC, Sigma) and N-hydroxysulfosuccinimide (NHSS, Sigma) were dissolved in water immediately before use. Immunoreagents were dissolved in pH 7.0 phosphate saline (PBS) buffer (0.01 M in phosphate, 0.14 M NaCl, 2.7 mM KCl) unless otherwise noted. Carboxyl functionalized magnetic beads were obtained from Polyscience, Inc.

Human serum samples were obtained from Capital Biosciences. Serum sample 1 was from a normal female control, and samples 2 and 3 were chosen from male patients with indications of prostate carcinoma, and clinically defined as having prostate carcinoma. HeLa and LNCaP cells (cervical and prostate specific cancers, respectively) were cultured in DMEM supplemented with 10% fetal bovine serum at 37°C in 95% air/5% CO_2. For lysate preparation, exponentially growing cells were lysed in T-PER (Tissue Protein Extraction Reagent; Pierce, IL, USA), and solubilized complex proteins were cleared by centrifugation and stored at −80° C until use.

Instrumentation

A CHI 660 electrochemical workstation was used for cyclic voltammetry and amperometry at ambient temperature (22 ± 2 °C) in a three electrode cell. Amperometry was done at −0.3 V vs SCE with the AuNP working electrode rotated at 3000 rpm for optimum sensitivity. A nanoscope IV multimode atomic force microscope was used for the characterization of the AuNP platform. A USI (Japan) quartz crystal microbalance (QCM) employing 9 MHz QCM resonators (AT-cut, International Crystal.) as used to measure film weights.

Synthesis of Glutathione protected AuNPs (GSH-AuNPs)

Glutathione protected AuNPs with diameter 5 nm were prepared by the reduction of gold salt using sodium borohydride in the presence of glutathione[45] as illustrated in Scheme 1. In brief, a quantity of 19.7 mg $HAuCl_4.3H_2O$ and 7.7 mg of glutathione were added to a mixture of solvents, methanol (3.0 mL) and acetic acid (0.5 mL) and dissolved by stirring for 5 min, resulting in a clear yellow solution. Sodium borohydride solution was prepared by dissolving 30 mg of $NaBH_4$ in 1.5 g of nanopure water. The $NaBH_4$ solution was added dropwise into above solution with rapid stirring. The color of $HAuCl_4$ changed from yellow to brown upon addition of $NaBH_4$ solution. Rapid stirring was continued for 2 h. The glutathione protected gold nanoparticles (GSH-AuNP) thus formed were soluble in water.

The particle solution was filtered through a 50KDa MW cutoff, centrifuging at 3500 rpm and washed with nanopure water for 4 times, and then dissolved in 20 mM HEPES buffer at pH 8.0. The resulting particles were characterized by transmission electron microscopy and plasmon resonance spectra and found to 5.05±1.4 nm in diameter.

Fabrication of AuNP electrode

AuNP electrodes were prepared by layer-by-layer assembly of layers of poly (diallydimethylammonium chloride) (PDDA) and the AuNPs on pyrolytic graphite (PG) or mica for characterization.[44] In brief, 20 μL of PDDA solution (2 mg mL^{-1}, containing 0.05 M NaCl) was placed on a PG disk (A=0.14 cm^2) surface for 20 min to adsorb positively charged PDDA as a precursor layer. After washing with water, 20 μL of 2 mg mL^{-1} of GSH-AuNPs was placed on this electrode for 20 min to adsorb the negatively charged GSH-AuNP layer. Water washing and drying nitrogen stream resulted in the final PDDA/GSH-AuNP bilayer on the PG surface.

Immobilization of proteins

For HRP immobilization, 20 μL of freshly prepared 24 mM EDC in water was placed onto the AuNP electrode, followed by 20 μL of 3 mg/mL HRP, reacted for 8 h, washed with water. For capture antibody attachment, 30 μL of freshly prepared 400 mM EDC and 100 mM NHSS in water was placed onto AuNP electrodes for 10 min, and washed off with water, followed by 3 h incubation with 20 μL of 330 μg/mL of primary anti-human prostate specific antigen (PSA) antibody in pH 7.0 PBS buffer containing 0.05 % Tween-20. Unbound antibody was removed by rinsing thoroughly with PBS (7.0) Tween-20 and PBS buffer for 3 minutes each.

Fabrication and use of AuNP Immunosensors

Onto immunosensors prepared as described above was placed 10 μL of casein (0.4% w/v) in PBS Tween-20 to stand for 1 h at room temperature to block free antibody binding sites on the surface. Afterwards the electrodes were rinsed thoroughly with PBS Tween-20, then PBS buffer for 3 minutes each. Then 10 μL of the PSA standard solution in undiluted calf serum or human serum or cell lysates were incubated on the sensor surface for 1.25 h at room temperature. After several PBS washing steps the electrodes were exposed to 20 μL of 4 pmol mL^{-1} Ab_2-HRP in buffer containing 0.4% casein and 0.05% Tween-20 or to Ab_2-magnetic bead-HRP conjugates in buffer containing 0.05 % Tween-20 for a further 1.25 h. These sensors were rinsed thoroughly with PBS-Tween 20 and PBS buffer, then placed in an electrochemical cell containing PBS buffer with 1 mM hydroquinone, holding applied potential at −0.3 V and rotating at 3000 rpm, then injecting H_2O_2 to 0.4 mM for Ab_2-HRP and 0.04 mM for Ab_2-magnetic bead- HRP while measuring the amperometric current.

The serum and cell lysate samples were analyzed by a referee ELISA as method by using Human PSA ELISA Kit (Catalogue No. EL10005, 96 well plate) from Anogen.

Preparation of Ab_2-magnetic bead-HRP bioconjugates

2 mg of carboxyl functionalized 1 μm diameter magnetic beads (Polysciences) were dispersed in 1 mL 50 mM MES buffer at pH 5.2. This dispersion was then mixed with 3.2 mg of EDC and vortexed at room temperature for 5 min. The resulting mixture was magnetically separated and supernatant was discarded and washed with 50 mM MES buffer. Detection anti-PSA antibody (Ab_2, 0.01 mg mL^{-1}) and 1.2 mg mL^{-1} HRP were added to the mixture and stirred on a non-magnetic mixing device for 16 h at room temperature. The reaction mixture was magnetically separated by placing a magnet under the bottom of the reaction vessel, and the supernatant was discarded. The particles were resuspended in 1 mL 1 M Glycine at pH 8.0 and vortexed for 30 min. The resulting mixture was washed with pH 7.0 PBS buffer 3–4 times and later dispersed in 400 μL of pH 7.0 PBS buffer + 0.05% Tween-20. The bioconjugate thus obtained was diluted 5 times with PBS-Tween 20 before use.

Supplementary Material

Refer to Web version on PubMed Central for supplementary material.

Acknowledgement

This research was supported by PHS grant ES013557 from NIEHS/NIH, and by the intramural programs of the National Institute of Dental and Craniofacial Research, NIH. We thank Joseph D. Gong for TEM analysis, and Debra Rood and Lawrence K. Silbart for assistance with ELISA measurements.

REFERENCES AND NOTES

1. Schmid G. Large Clusters and Colloids. Metals in the Embryonic State. Chem. Rev 1992;92:1709–1727.
2. Shipway AN, Katz E, Willner I. Nanoparticle Arrays on Surfaces for Electronic, Optical, and Sensor Applications. ChemPhysChem 2000;1:18–52.
3. Daniel M-C, Astruc D. Gold Nanoparticles: Assembly, Supramolecular Chemistry, Quantum-Size-Related Properties, and Applications toward Biology, Catalysis, and Nanotechnology. Chem. Rev 2004;104:293–346. [PubMed: 14719978]
4. Gittins DI, Bethell D, Schiffrin DJ, Nichols RJ. A Nanometer-Scale Electronic Switch consisting of a Metal Cluster and Redox-addressable Groups. Nature 2000;408:67–69. [PubMed: 11081506]
5. Templeton AC, Wuelfing WP, Murray RW. Monolayer-Protected Cluster Molecules. Acc. Chem. Res 2000;33:27–36. [PubMed: 10639073]
6. Sanchez A, Abbet S, Heiz U, Schneider W-D, Häkkinen H, Barnett RN, Landman U. When Gold is not Noble: Nanoscale Gold Catalysts. J. Phys. Chem. A 1999;103:9573–9578.
7. Haruta M. Size- and Support-Dependency in the Catalysis of Gold. Catal. Today 1997;36:153–166.
8. Wangoo N, Suri CR, Shekhawat G. Interaction of Gold Nanoparticles with Protein: A Spectroscopic Study to Monitor Protein Conformational Changes. Appl. Phys. Lett 2008;92:133104-1–133104-3.
9. Mandal S, Phadtare S, Sastry M. Interfacing Biology with Nanoparticles. Curr. Appl. Phys 2005;5:118–127.
10. Wark AW, Lee HJ, Qavi AJ, Corn RM. Nanoparticle-Enhanced Diffraction Gratings for Ultrasensitive Surface Plasmon Biosensing. Anal. Chem 2007;79:6697–6701. [PubMed: 17676761]
11. Li D, Yan Y, Wieckowska A, Willner I. Amplified Electrochemical Detection of DNA through the Aggregation of Au Nanoparticles on Electrodes and the Incorporation of Methylene Blue into the DNA-Crosslinked Structure. Chem. Commun 2007:3544–3546.
12. Wei H, Li B, Li J, Wang E, Dong S. Simple and Sensitive Aptamer-Based Colorimetric Sensing of Protein using Unmodified Gold Nanoparticle Probes. Chem. Commun 2007:3735–3737.
13. Lee J-S, Han MS, Mirkin CA. Colorimetric Detection of Mercuric Ion (Hg^{+2}) in Aqueous Media using DNA-Functionalized Gold Nanoparticles. Angew. Chem. Int. Ed 2007;46:4093–4096.
14. Jensen PS, Chi Q, Grumsen FB, Abad JM, Horsewell A, Schiffrin DJ, Ulstrup J. Gold Nanoparticle Assisted Assembly of a Heme Protein for Enhancement of Long-Range Interfacial Electron Transfer. J. Phys. Chem. C 2007;111:6124–6132.
15. Yi X, Huang-Xian J, Hong-Yuan C. Direct Electrochemistry of Horseradish Peroxidase Immobilized on a Colloid/Cysteamine-Modified Gold Electrode. Anal. Biochem 2000;278:22–28. [PubMed: 10640349]
16. Zhang H, Lu H, Hu N. Fabrication of Electroactive Layer-by-Layer Films of Myoglobin with Gold Nanoparticles of Different Sizes. J. Phys. Chem. B 2006;110:2171–2179. [PubMed: 16471801]
17. Zhao S, Zhang K, Bai Y, Yang W, Sun C. Glucose Oxidase/Colloidal Gold Nanoparticles Immobilized in Nafion Film on Glassy Carbon Electrode: Direct Electron Transfer and Electrocatalysis. Bioelectrochem 2006;69:158–163.
18. Xiao Y, Patolsky F, Katz E, Hainfeld JF, Willner I. “Plugging into Enzymes”: Nanowiring of Redox Enzymes by a Gold Nanoparticle. Science 2003;299:1877–1881. [PubMed: 12649477]

19. Zayats M, Katz E, Baron R, Willner I. Reconstitution of Apo-Glucose Dehydrogenase on Pyrroloquinoline Quinone-Functionalized Au Nanoparticles Yields an Electrically Contacted Biocatalyst. J. Am. Chem. Soc 2005;127:12400–12406. [PubMed: 16131222]
20. Shipway AN, Lahav M, Willner I. Nanostructured Gold Colloid Electrodes. Adv. Mater 2000;12:993–998.
21. Murphy L. Biosensors and Bioelectrochemistry. Curr. Opin. Chem. Biol 2006;10:177–184. [PubMed: 16516536]
22. Guo S, Wang E. Synthesis and Electrochemical Applications of Gold Nanoparticles. Anal. Chim. Acta 2007;598:181–192. [PubMed: 17719891]
23. Singh K, Rahman A, Son JI, Kim KC, Shim Y-B. An Amperometric Immunosensor for Osteoproteogerin based on Gold Nanoparticles Deposited Conducting Polymer. Biosens. Bioelectron 2008;23:1595–1601. [PubMed: 18304799]
24. Smith JC, Lambert J-P, Elisma F, Figeys D. Proteomics in 2005/2006: Developments, Applications and Challenges. Anal. Chem 2007;79:4325–4344. [PubMed: 17477510]
25. Kitano H. Systems Biology: A Brief Overview. Science 2002;295:1662–1664. [PubMed: 11872829]
26. Hood E. Proteomics Characterizing the Cogs in the Machinery of Life. Environ. Health Perspect 2003;111:A817–A825.
27. Bensalah K, Lotan Y, Karam JA, Shariat SF. New Circulating Biomarkers for Prostate Cancer. Prostate Cancer Prostatic. Dis 2008;11:112–120. [PubMed: 17998918]
28. Voller A, Bartlett A, Bidwell DE. Enzyme Immunoassays with Special Reference to ELISA Techniques. J. Clin. Pathol 1978;31:507–520. [PubMed: 78929]
29. Goldsmith SJ. Radioimmunoassay: Review of Basic Principles. Semin. Nucl. Med 1975;5:125–152. [PubMed: 164695]
30. Schmalzing D, Nashabeh W. Capillary Electrophoresis based Immunoassays: A Critical Review. Electrophoresis 1997;18:2184–2193. [PubMed: 9456033]
31. Aebersold R, Mann M. Mass Spectrometry-based Proteomics. Nature 2003;422:198–207. [PubMed: 12634793]
32. Xiao Z, Prieto D, Conrads TP, Veenstra TD, Issaq HJ. Proteomics Patterns: their Potential for Disease Diagnosis. Mol. Cell. Endocrinol 2005;230:95–106. [PubMed: 15664456]
33. Weston AD, Hood L. Systems Biology, Proteomics, and the Future of Health Care: Toward Predictive, Preventative, and Personalized Medicine. J. Proteome Res 2004;3:179–196. [PubMed: 15113093]
34. Wagner PD, Verma M, Srivastava S. Challenges for Biomarkers in Cancer Detection. Ann. N. Y. Acad. Sci 2004;1022:9–16. [PubMed: 15251933]
35. Yu X, Kim SN, Papadimitrikopoulos F, Rusling JF. Protein Immunosensor using Single-Wall Carbon Nanotube Forests with Electrochemical Detection of enzyme Labels. Mol. Biosyst 2005;1:70–78. [PubMed: 16880966]
36. Wu G, Datar RH, Hansen KM, Thundat T, Cote RJ, Majumdar A. Bioassay of Prostate-Specific Antigen (PSA) using Microcantilevers. Nat. Biotechnol 2001;19:856–860. [PubMed: 11533645]
37. Zheng G, Patolsky F, Cui Y, Wang WU, Lieber CM. Multiplexed electrical detection of cancer markers with nanowire sensor arrays. Nat. Biotechnol 2005;23:1294–1301. [PubMed: 16170313]
38. Alivisatos P. The Use of Nanocrystals in Biological Detection. Nat. Biotechnol 2004;22:47–52. [PubMed: 14704706]
39. Lilja H, Ulmert D, Vickers AJ. Prostate-Specific Antigen and Prostate Cancer: Prediction, Detection and Monitoring. Nature Rev. Cancer 2008;8:268–278. [PubMed: 18337732]
40. Yu X, Munge B, Patel Y, Jensen G, Bhirde A, Gong JD, Kim SN, Gillespie J, Gutkind JS, Papadimitrakopoulos F, Rusling JF. Carbon Nanotubes Amplification Strategies for Highly Sensitive Immunodetection of Cancer Biomarkers. J. Am. Chem. Soc 2006;128:11199–11205. [PubMed: 16925438]
41. Chattopadhyay D, Galeska I, Papadimitrakopoulos F. Metal-Assisted Organization of Shortened Carbon Nanotubes in Monolayer and Multilayer Forest Assemblies. J. Am. Chem. Soc 2001;123:9451–9452. [PubMed: 11562232]
42. Kim SN, Rusling JF, Papadimitrakopoulos F. Carbon Nanotubes for Electronic and Electrochemical Detection of Biomolecules. Adv. Mater 2007;19:3214–3228.

43. Rusling, JF. Electroactive and enzyme-active protein polyion films assembled layer-by-layer. In: Lvov, Y.; Mohwald, H., editors. Protein Architecture: Interfacing Molecular Assemblies and Immobilization Biotechnology. New York: Marcel Dekker; 2000. p. 337-354.
44. Lvov, YM. Thin-film nanofabrication by alternate adsorption of polyions, nanoparticles, and proteins. In: Nalwa, HS., editor. Handbook of Surfaces and Interfaces of Material : Nanostructured Materials, Micelles, and Colloids. Vol. Vol. 3. San Diego: Academic Press; 2001. p. 170-189.
45. Zheng M, Huang X. Nanoparticles Comprising a Mixed Monolayer for Specific Bindings with Biomolecules. J. Am. Chem. Soc 2004;126:12047–12054. [PubMed: 15382939]
46. (a) Riedel F, Zaiss I, Herzog D, Götte K, Naim R, Hörman. Serum Levels of Interleukin 6 in Patients with Primary heady and Neck Squamous Cell Carcinoma. Anticancer Res 2005;25:2761–2766. [PubMed: 16080523] (b) Williams TI, Toups KL, Saggese DA, Kalli KR, Cliby WA, Muddiman DC. Epithelial Ovarian Cancer: Disease Etiology, Treatment, Detection, and Investigational Gene, Metabolite, and Protein Biomarkers. J. Proteome Res 2007;6:2936–2962. [PubMed: 17583933]
47. Haiss W, Thanh NTK, Aveyard J, Fernig DG. Determination of Size and Concentration of Gold Nanoparticles from UV-Vis Spectra. Anal. Chem 2007;79:4215–4221. [PubMed: 17458937]
48. Zhou L, Rusling JF. Detection of Chemically Induced DNA Damage in Layered Films by Catalytic Square Wave Voltammetry Using $Ru(bpy)_3^{2+}$ Anal. Chem 2001;73:4780–4786. [PubMed: 11681451]
49. Henz BJ, Hawa T, Zachariah MR. Mechano-Chemical Stability of Gold Nanoparticles Coated with Alkanethiolate SAMs. Langmuir 2008;24:773–783. [PubMed: 18189429]
50. Ruzgas, T.; Lindgren, A.; Gorton, L.; Hecht, H-J.; Reichelt, J.; Bilitewski, U. Electrochemistry of Peroxidases. In: Chambers, JQ.; Brajter-Toth, A., editors. Electroanalytical Methods for Biological Materials. New York: Marcel Dekker; 2002. p. 233-254. (b) Zhang Z, Chouchane S, Magliozzo RS, Rusling JF. Direct Voltammetry and Catalysis with Mycobacterium tuberculosis Catalase-Peroxidase, Peroxidases and Catalase in Lipid Films. Anal. Chem 2002;74:163–170. [PubMed: 11795785]
51. Rusling, JF.; Zhang, Z. Designing functional biomolecular films on electrodes. In: Rusling, JF., editor. Biomolecular Films. N. Y.: Marcel Dekker; 2003. p. 1-64.
52. Carter HB, Isaacs WB. Improved Biomarkers for Prostate Cancer: A Definite Need. J. Natl. Cancer Inst 2004;96:813–815. [PubMed: 15173257]
53. Gallati H. Horseradish Peroxidase: A Study of the Kinetics and the Determination of Optimal Reaction Conditions, using Hydrogen Peroxide and 2,2'- azinobis 3-ethylbenzthiazoline-6-sulfonic acid (ABTS) as Substrates. J. Clin. Chem. Clin. Biochem 1979;17:1–7. [PubMed: 33227]
54. Healy DA, Hayes CJ, Leonard P, McKenna L, O'Kennedy R. Biosensor Developments: Application to Prostate-Specific Antigen Detection. Trends Biotechnol 2007;25:125–131. [PubMed: 17257699]
55. Gkonos PJ, Guo F, Burnstein KL. Type I Vasoactive Intestinal Peptide Receptor Expression in PC3/AR Cells Is Evidence of Prostate Epithelial Differentiation. The Prostate 2000;42:137–144. [PubMed: 10617871]
56. Mckiernan JM, Buttyan R, Bander NH, Stifelman MD, Katz AE, Chen M, Olsson CA, Sawczuk IS. Expression of the Tumor-associated Gene MN: A Potential Biomarker for Human Renal Cell Carcinoma. Cancer Res 1997;57:2362–2365. [PubMed: 9192809]
57. Woodrum DL, French CM, Hill TM, Roman SJ, Slatore HL, Shaffer JL, York LG, Eure KL, Loveland KG, Gasior GH, et al. Analytical Performance of the Tandem R free PSA Immunoassay measuring free prostate-specific antigen. Clin. Chem 1997;43:1203–1208. [PubMed: 9216457]
58. Dnistrian AM, Schwartz MK, Smith CA, Nisselbaum JS, Fair WR. Abbott IMx Evaluated for Assay of Prostate Specific Antigen in Serum. Clin. Chem 1992;38:2140–2142. [PubMed: 1382898]
59. Mora-Brugues J, Gascon-Roche N, Rodriguez-Espinosa J, Cortes-Rius M, Gonzalez-Sastre F. Evaluation of Ciba Corning ACS: 180™ Automated Immunoassay System. Clin. Chem 1994;40:407–410. [PubMed: 7510590]
60. Ward MA, Catto JWF, Hamdy FC. Prostate Specific Antigen: Biology, Biochemistry and Availaible Commerical Assays. Ann. Clin. Biochem 2001;38:633–651. [PubMed: 11732646]
61. Kim A, Ah CS, Yu HY, Yang J-H, Baek I-B, Ahn C-G, Park CW, Jun MS. Ultrasensitive, Label-Free, and Real Time Immunodetection using Silicon Field-Effect Transistors. Appl. Phys. Lett 2007;91:103901-1–103901-3.

62. Choi J-W, Oh B-K, Jang Y-K, Kang D-Y. Ultrasensitive Immunoassay for Prostate Specific Antigen using Scanning Tunneling Microscopy- Based Electrical Detection. Appl. Phys. Lett 2008;93:033110-1–033110-3.

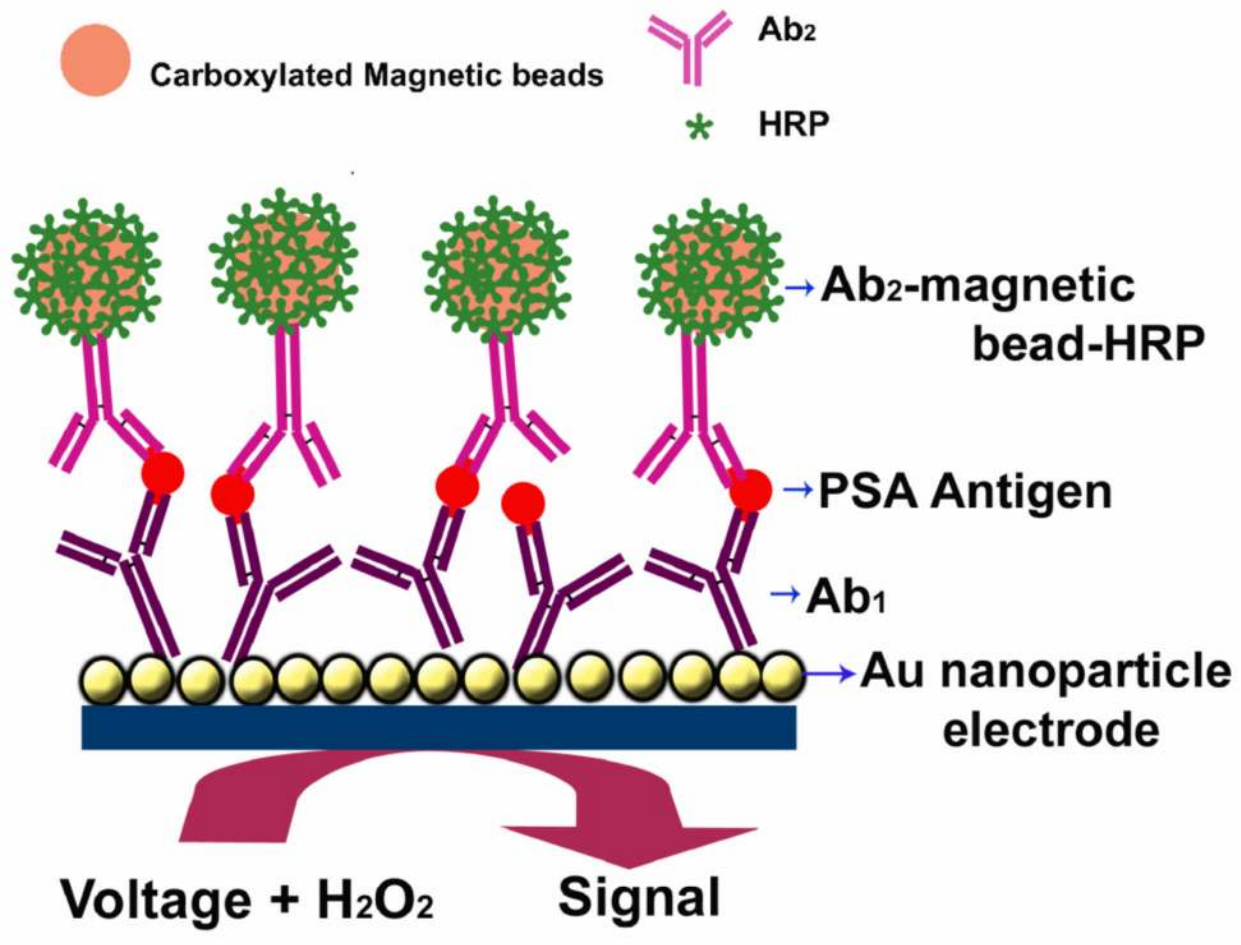

Figure 1.

AuNP immunosensor with Ab_1 attached that has captured an antigen from a sample after treating with Ab_2- magnetic bead-HRP providing multiple enzyme labels for each PSA. The detection step involves immersing the immunosensor into buffer containing mediator, applying voltage, and injecting H_2O_2.

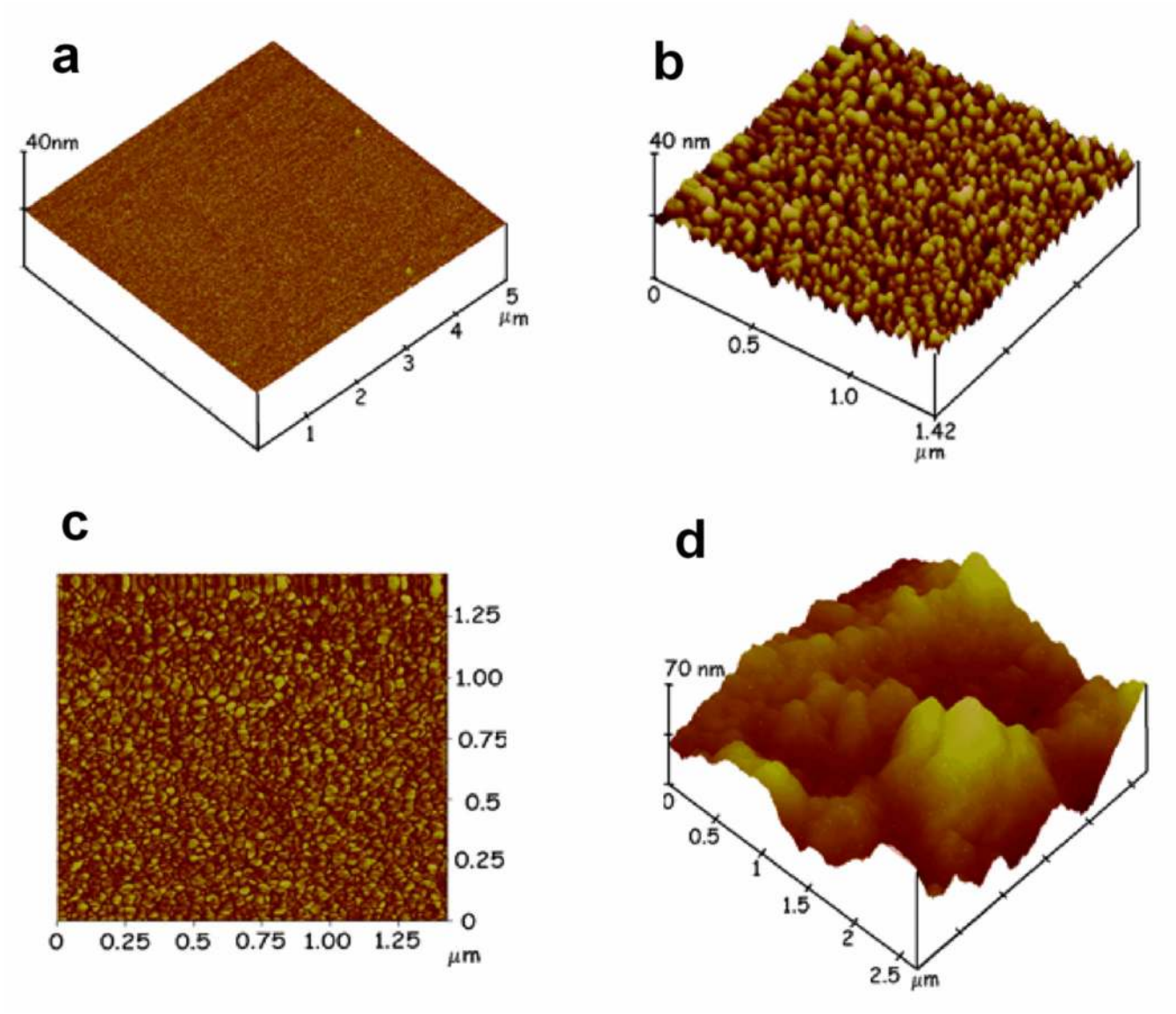

Figure 2.

Tapping mode atomic force microscope images of a) layer of PDDA on smooth mica surface; b) PDDA/AuNP bilayer; c) phase contrast image of PDDA/AuNP bilayer; d) AuNP platform after covalent linkage of anti-PSA antibodies onto the glutathione carboxylate groups of AuNP.

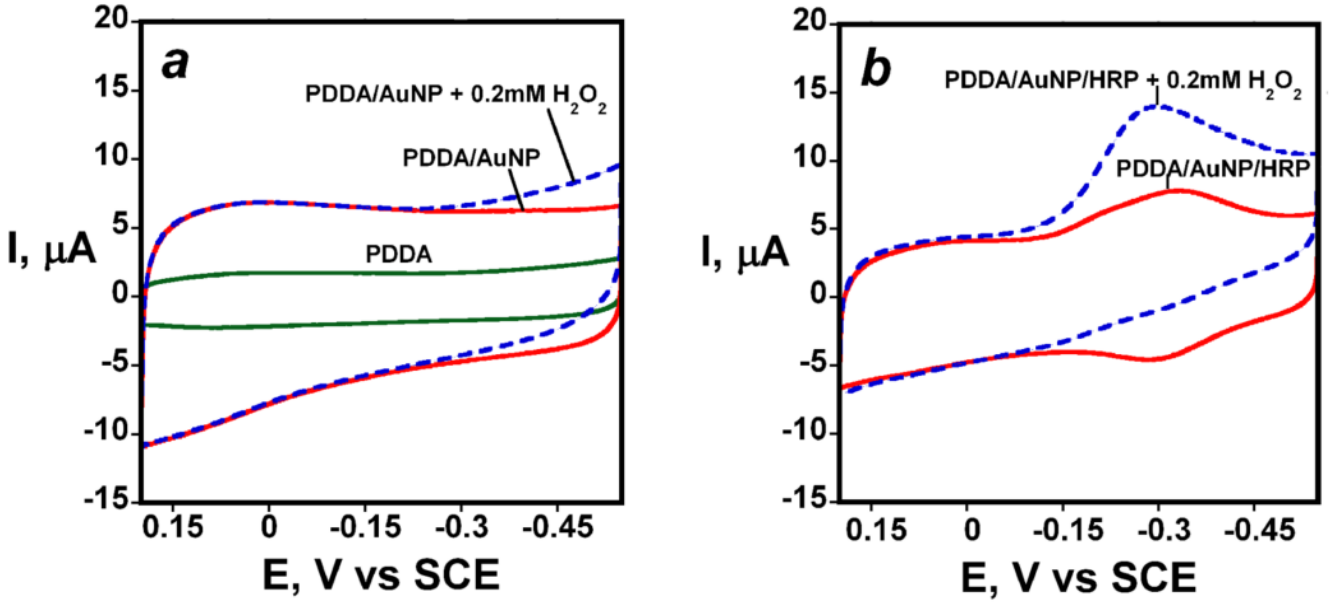

Figure 3.

Cyclic voltammograms at 300 mV s^{-1} in pH 6.5 phosphate buffer for: (a) PDDA film, PDDA/AuNP on electrode with and without 0.2 mM H_2O_2 (b) PDDA/AuNP/HRP with and without 0.2 mM H_2O_2

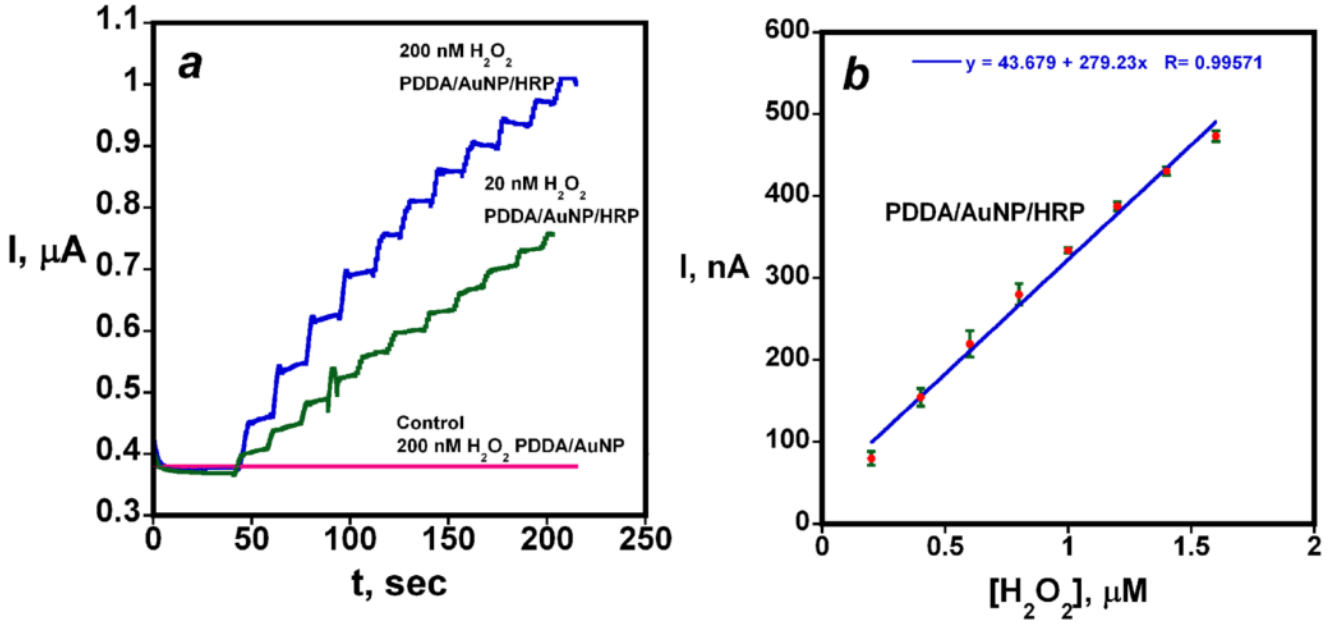

Figure 4.

Catalytic electrochemical reduction of hydrogen peroxide on HRP/AuNP electrodes from rotating disk amperometry at −0.2 V vs SCE and 2000 rpm: (a) showing 20 and 200 nM increases in H_2O_2 concentration by aliquot injection into the solution; (b) calibration plot for peroxide from rotating disk amperometry (n=3 electrodes).

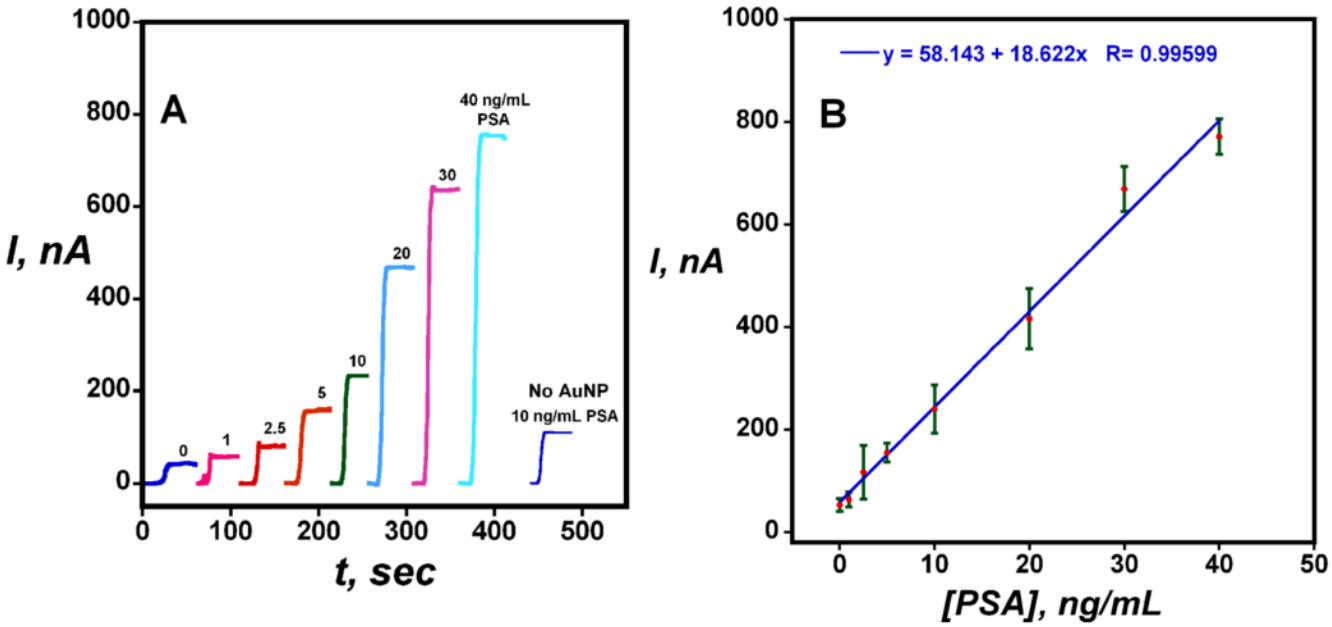

Figure 5.

Amperometric results for AuNP immunosensors incubated with PSA in 10 μL undiluted calf serum for 1.25 h followed by 4 pmol mL^{-1} conventional Ab_2-HRP in 10 μl 0.4 % w/v casein and 0.05 % tween 20 PBS buffer for 1.25 h: (A) steady state amperometric current at −0.3 V and 3000 rpm after placing electrodes in buffer containing 1 mM hydroquinone and, then injecting H_2O_2 to 0.4 mM. the "No AuNP" control response corresponds to Immunosensors built on PDDA coated PG electrodes at 10 ng mL^{-1} PSA; (B) Immunosensor calibration plot for PSA (n= 3).

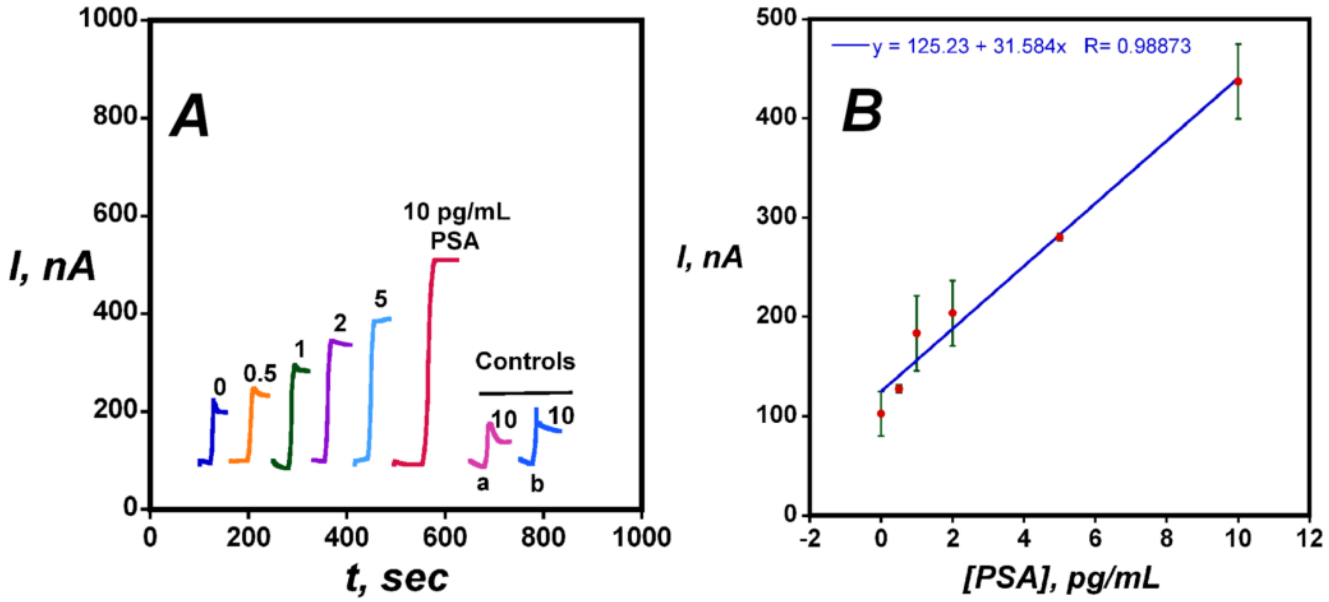

Figure 6.

Amperometric results for AuNP immunosensors incubated with PSA in 10 μL undiluted calf serum for 1.25 h followed by multilabel Ab_2-magnetic bead- HRP in 10 μL 0.05 % Tween 20 PBS buffer for 1.25 h: (A) steady state amperometric current at −0.3 V and 3000 rpm after placing electrodes in PBS buffer containing 1 mM hydroquinone and, then injecting 0.04 mM H_2O_2. (a) Immunosensors built on bare PG surface at 10 pg mL^{-1} PSA (b) Immunosensors built on PDDA coated with PG surface at 10 pg mL^{-1} PSA; (B) Immunosensor calibration plot for PSA (n= 3)

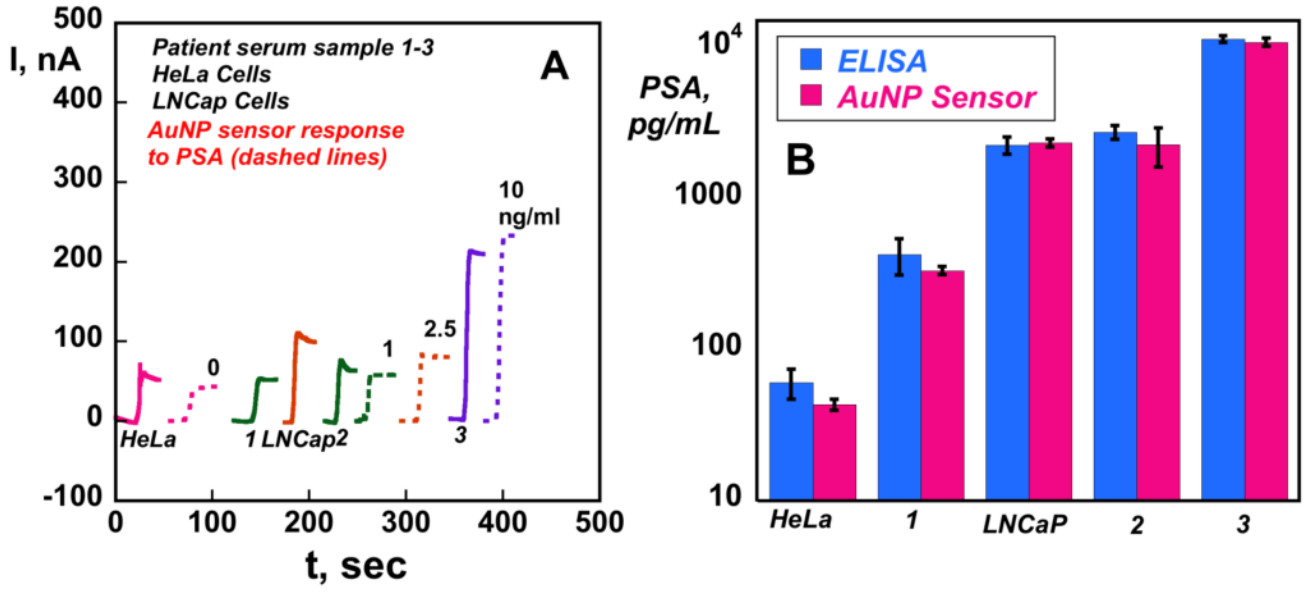

Figure 7.

Results for AuNP immunosensors incubated with PSA in 10 μL calf serum (ng/mL labeled on curves, dashed lines), cell lysates (HeLa and LNCaP Cells) and human patient serum samples (1–3) (solid lines) for 1.25 h followed by 10 μL 4 pmol mL^{-1} anti-PSA-HRP in 0.4 % casein and 0.05 % tween-20 for 1.25 h: (A) amperometric current at −0.3 V and 3000 rpm using 1 mM hydroquinone mediator, then injecting H_2O_2 to 0.4 mM; (B) Validation of AuNP sensor results for cell lysate and human serum samples by comparing against results from ELISA determination (RSD ± 10%) for same samples.

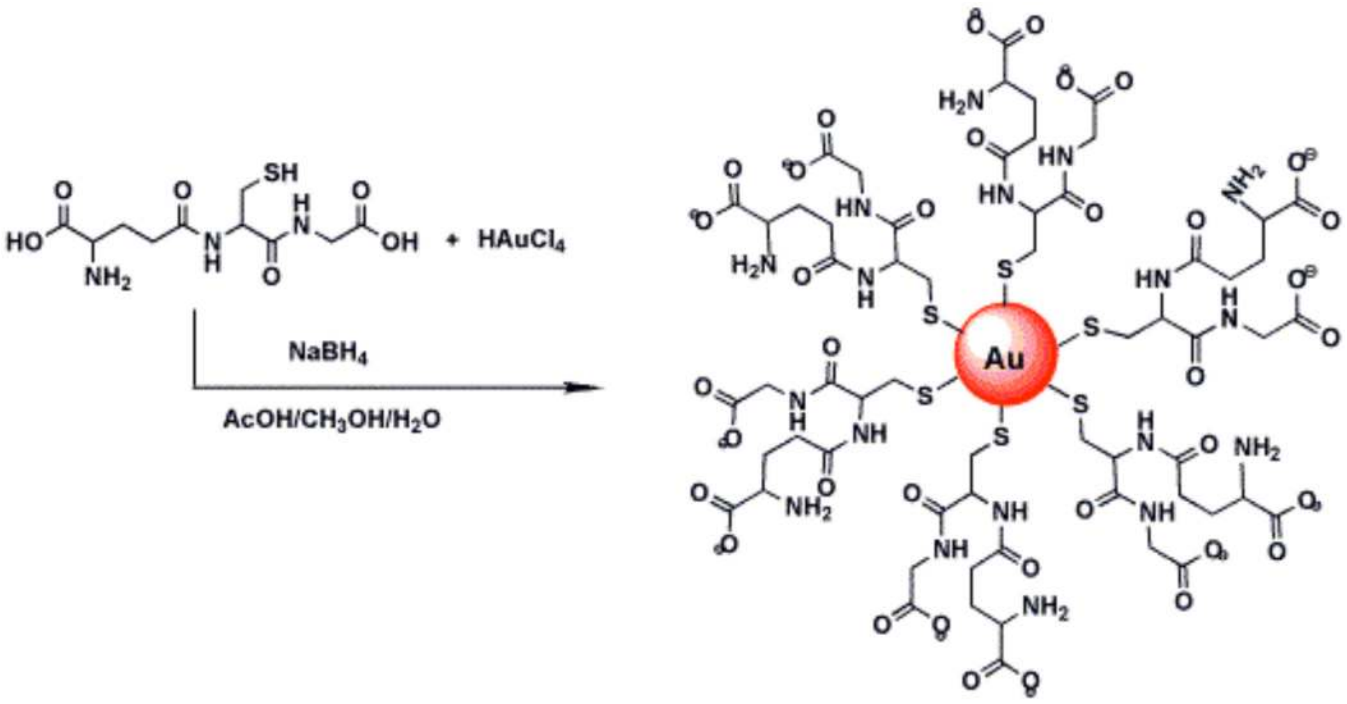

Scheme 1.
Synthesis of glutathione protected gold nanoparticles

Table 1

Average characteristics of AuNP film obtained from QCM data

Mass of AuNP film per unit area	2.42 ± 0.36 μg cm^{-2}
No. of AuNPs adsorbed	4.1×10^{11}
Nominal thickness of AuNP film	7.1 ± 1.0 nm
Nominal thickness of PDDA film	0.26 ± 0.17 nm
Nominal surface coverage	>75 %[a]

[a]Based on density of bulk gold, but larger if density is less than bulk gold.[49]